PERGAMON

International Journal of Heat and Mass Transfer 45 (2002) 2397–2405

International Journal of HEAT and MASS TRANSFER

www.elsevier.com/locate/ijhmt

Mushy zone equilibrium solidification of a semitransparent layer subject to radiative and convective cooling

Chengcai Yao, B.T.F. Chung *, G.-X. Wang

Department of Mechanical Engineering, University of Akron, Akron, OH 44325-3903, USA

Received 8 August 2000; received in revised form 10 March 2001

Abstract

Equilibrium solidification in a semitransparent planar layer is studied using an isothermal mushy zone model. The layer is made up of a pure material being emitting, absorbing and isotropically scattering and is subject to radiative and convective cooling. The model involves solving simultaneously the transient energy equation and the radiation transport equation. An implicit finite volume scheme is employed to solve the energy equation, with the discrete ordinate method being used to deal with the radiation transport. A systematical parametric study is performed and the effects of various materials optical properties and processing conditions are investigated. It is found that decreasing the optical thickness and increasing the scattering albedo both lead to a wider mushy zone and a slower rate of solidification.

1. Introduction

Melting and solidification of semitransparent materials are important physical phenomena involved in many engineering areas such as crystal growth, laser material processing, and nuclear engineering. The problem becomes extremely challenging because of complex radiation heat transfer with internal absorbing, emitting and scattering [1–3]. O'Hara et al. [4] were the first to treat solidification of a pure semitransparent material by explicitly taking into account the internal radiation. They solved a one-dimensional, steady-state, planar interface solidification problem. Their analysis indicates that internal radiation significantly alters the temperature distributions in the melt and solid and thus affects the stability of the planar interface. Later, Abrams and Viskanta [5] extended this work by including the transient effect. An important finding of their work is the melt supercooling in front of interface induced by the internal radiation. Such melt undercooling may destabilize the planar interface and thus leads to cellular or dendritic structure, i.e., a mushy zone. Vasil'ev and Yuferev [6,7] also observed such melt supercooling in studying shaped growth of thin sapphire crystal which is a semitransparent material. This phenomenon was referred to as "radiative supercooling". Habib [8] analyzed the melting process of a one-dimensional slab earlier but did not observe the melt supercooling since the heat balance integral method with an assumed temperature profile was employed.

Planar interface model has been assumed in many following analyses with the effect of scattering being considered. For example, Seki et al. [9] used a finite difference method to study back melting of an ice layer immediately adjacent to a surface. The ice was assumed to be non-gray, isotropically scattering but non-emitting. Cho and Ozisik [10] also considered the effect of isotropic scattering in their study of one-dimensional solidification of a semi-infinite medium. Diaz and Viskanta [11], on the other hand, utilized a non-gray model to investigate the melting of an *n*-octadecane slab due to an external radiation source. Highly peaked forward scattering was assumed for the radiation problem but the radiation from the medium was neglected. Extensive efforts were also made to study the effect of internal radiation in various growth processes of oxide crystals (see [3,12,13]). Here multi-dimensional geometries were considered.

Since the undercooled melt is a thermodynamic metastable phase, it would be difficult to sustain a large

* Corresponding author. Tel.: +330-972-7739; fax: +330-972-2011.

E-mail address: bchung@uakron.edu (B.T.F. Chung).

0017-9310/02/$ - see front matter
PII: S0017-9310(01)00333-7

Nomenclature

c	specific heat of the material (J/kg K)
D	thickness of the medium (m)
h	enthalpy (J/kg)
h_c	convective heat transfer coefficient (W/m^2 K)
H	dimensionless enthalpy, $(h - cT_m)cT_m$
H_R	convection–radiation parameter, $h_c/(\sigma T_m^3)$
k	thermal conductivity of the medium (W/m K)
n	refractive index of the medium
N	conduction–radiation parameter, $k/(4\sigma T_m^3 D)$
q_r	radiative heat flux (W/m^2)
$\bar{q}_r$	dimensionless radiative heat flux, $q_r/(4\sigma T_m^4)$
St	Stefan number, cT_m/λ
t	time (s)
T	absolute temperature (K)
T_0	initial temperature (K)
T_e	temperature of the environment (K)
T_m	freezing temperature (K)
x	coordinate in direction across the slab (m)
X	dimensionless coordinate, x/D

Greek symbols

β	extinction coefficient of the medium (m^{-1})
θ	dimensionless temperature, T/T_m
κ_D	optical thickness of the layer, βD
λ	latent heat of fusion (J/kg)
ρ	density (kg/m^3)
ρ^0, ρ^i	reflectivities to external and internal incidence
σ	Stefan–Boltzmann constant (5.6705×10^{-8} W/m^2 K^4)
τ	dimensionless time $(4\sigma T_m^3/\rho cD)t$
ω	single scattering albedo

undercooling in an engineering system, and instead, a two-phase region, i.e., a mushy zone, was suggested. The mushy zone may be made of either an equiaxed or a columnar structure depending on the solidification mechanisms [14]. If crystal nuclei are formed in the undercooled melt, they will grow in the zone and eliminate the melt undercooling. Chan et al. [15,16] were the first to propose such an isothermal mushy zone model, based on the assumption of local thermodynamic equilibrium condition that does not permit melt undercooling. On the other hand, the radiative supercooling would lead to the break down of the planar interface and an isothermal mushy zone would be formed made of thermal cells or dendrites [4,17]. With the assumption of local thermodynamic equilibrium in the mushy zone, for a pure material the mushy zone will be isothermal in both cases but with very different structures [14]. For some special cases with high rates of heat transfer and small geometric dimensions, the planar interface may be stable even with a large melt undercooling. A preliminary analysis of such a non-equilibrium solidification problem was recently given by the present authors [18] with the introduction of the solidification kinetics.

Several studies exist in the literature using the equilibrium mushy zone model to treat the phase change problems of semitransparent materials. For example, Oruma et al. [19] examined in detail the effects of anisotropic scattering on melting and solidification of a semitransparent semi-infinite medium. They solved the problem approximately using the integral method with a parabolic temperature profile in the melt (for melting) but a constant temperature in the mushy zone and the remaining solid, and found a strong effect of anisotropic scattering on melting rates. The equilibrium mushy zone model has also been employed in the analyses of melting and ablation of semitransparent materials subject to a continuous [20] or a pulsed [21] laser irradiation.

The purpose of this study is to extend the earlier works of Chan et al. [15,16] by including the effects of optical thickness, heat conduction, scattering and external convection on the propagation of mushy zone in a pure semitransparent material. Furthermore, it is intended to present a comprehensive and systematical study on the mushy zone equilibrium solidification of semitransparent material with internal emitting, absorbing, and isotropic scattering. None of these results have been previously available in the open literature.

2. Mathematical formulation and numerical solution

Consideration is given to a plane layer of thickness D, as shown in Fig. 1, made of a gray medium being emitting, absorbing, and isotropically scattering. The slab is initially at temperature T_0 above the freezing

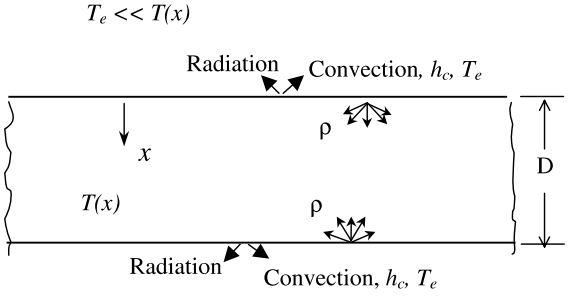

Fig. 1. Schematic of a semitransparent slab placed in a cold environment.

point of the material, and is placed in a much colder surrounding. The slab surfaces are subject to both radiation and external convective cooling. To simplify the analysis, all properties are assumed to be temperature-independent and phase-independent. Since the heat transfer conditions from both surfaces of the slab are assumed to be the same, only half of the slab will be analyzed. Using the dimensionless variables defined in the nomenclature, we can write the conservation of energy equation as

$$\frac{\partial H}{\partial \tau} = N\frac{\partial^2 \theta}{\partial X^2} - \frac{\mathrm{d}\bar{q}_\mathrm{r}}{\mathrm{d}X}. \tag{1}$$

The dimensionless temperature, θ, and enthalpy, H, are related to each other by

$$\theta = \begin{cases} H+1 & \text{solid region,} & H<0, \\ 1 & \text{mushy region,} & 0 \leqslant H \leqslant 1/St, \\ H+1-1/St & \text{liquid region,} & H>1/St, \end{cases} \tag{2}$$

where St is the Stefan number. Eqs. (1) and (2) form the enthalpy formulation of the phase-change problem. This formulation is particularly convenient when there is a two-phase region. The local liquid fraction in the mushy zone is equal to the ratio of local enthalpy to that of saturated liquid phase; or one can easily write the solid fraction as $f_\mathrm{s} = 1 - H/(1/St)$.

It should be noted that, depending on the solidification mechanisms (equiaxed or columnar), the solid fraction f_s may have different physical explanations. In the present study, the model does not distinguish the structure configuration of the mushy zone in two solidification mechanisms, since both configurations give the same mathematical form of f_s, which is mainly controlled by the energy balance.

The gradient of the radiative heat flux in Eq. (1) can be found in standard texts [22,23]

$$\frac{\mathrm{d}\bar{q}_\mathrm{r}}{\mathrm{d}X} = \kappa_D(1-\omega)\left(n^2\theta^4 - \int_{4\pi}\bar{I}\,\mathrm{d}\Omega\right), \tag{3}$$

where the intensity of radiation, $\bar{I}$, can be solved from the radiative transfer equation (RTE). The RTE in a one-dimensional form can be written as

$$\frac{\xi}{\kappa_D}\frac{\mathrm{d}\bar{I}}{\mathrm{d}X} = -\bar{I} + (1-\omega)\frac{n^2\theta^4}{4\pi} + \frac{\omega}{4\pi}\int_{4\pi}\bar{I}(X,\Omega)\,\mathrm{d}\Omega, \tag{4}$$

where ξ is the direction cosine of a radiation ray.

At the surface of the slab ($X = 0$), the intensity of radiation can be written as [23]

$$\bar{I}(0,\Omega) = \frac{(1-\rho^0)\theta_\mathrm{e}^4}{4\pi} + \frac{\rho^i}{\pi}\int_{\xi<0}\bar{I}(0,\Omega)|\xi|\,\mathrm{d}\Omega \tag{5}$$

The surface is assumed to be diffusive and the reflectivities ρ^0 and ρ^i are determined by integrated averages from the Fresnel reflection relations [22]. At the center line ($X = 0.5$), the intensity is symmetrical.

Because the radiation passing through or reflected by the boundary has been taken into account in the solution of RTE, Eq. (4), the boundary condition for Eq. (1) only involves external convection

$$4N\frac{\partial\theta}{\partial X} = H_\mathrm{R}(\theta - \theta_\mathrm{e}) \quad \text{at } X = 0. \tag{6}$$

At the symmetry boundary,

$$\frac{\partial\theta}{\partial X} = 0 \quad \text{at } X = 0.5 \tag{7}$$

In Eq. (6), for convenience, we have assumed that the ambient temperature is the same as the environment temperature, θ_e.

The problem described above is solved using a fully implicit finite volume method [24], which involves solving the energy equation and the RTE iteratively. The latter is solved using the discrete ordinate (say, S_4) method [25]. It is found that a uniform grid with $\Delta X = 0.005$ (i.e., 101 nodes) gives grid independent results in terms of temperature and solid fraction distributions [26].

A mushy zone solidification process is typically characterized using the solid or liquid fraction distribution in the mushy zone. The boundary of the mushy region is defined as the imaginary division lines between the mushy region and pure solid or liquid regions. Knowledge of this boundary will be helpful in understanding the effect of internal radiation on the phase change process. The solid fraction in the mushy region decreases asymptotically away from the completely solidified portion, as has been pointed out by Chan et al. [15]. The boundary between the mushy region and the pure liquid region is defined as the location where the solid fraction $f_\mathrm{s} = 0.01$. Location of this boundary at each time increment can be found by interpolation when the distribution of solid fraction has been obtained from the enthalpy function.

The location of the boundary between the mushy region and the completely solidified region is determined as follows. Suppose at certain time, the front of the pure solid region is found within control volume i with enthalpy H_i. The enthalpy function in the mushy region (excluding this control volume) is then extrapolated to the ith node to give H_i', an apparent value representative of the enthalpy of the same control volume containing no pure solid region. The fraction of the mushy portion of the control volume i can now be approximated as H_i/H_i', because the enthalpy of the pure solid portion is zero. It follows that the position of the pure solid front is given by

$$X = 0.5(X_i + X_{i+1}) - H_i/H_i'. \tag{8}$$

The above approach generally yields a fairly smooth interface history curve.

In order to quantify the total solidification rate, we also define an imaginary total solid fraction interface that represents the total solidification fraction of the layer. Such a total fraction of solidified material includes the fractional solid in the mushy region as well as the pure solid region. Together with the solid boundary, it forms an envelope with its thickness reflecting the amount of solidified materials contained in the mushy zone.

3. Results and discussion

Solidification of a semitransparent material is controlled by many parameters, among which are the optical thickness, k_D, the conduction–radiation parameter, N, the scattering albedo, ω, and the external convective cooling coefficient, H_R. The ranges of these parameters are chosen among those proposed by Siegel [27]. For the results presented here, the refractive index, n, and the Stefan number, St, are held fixed, i.e., $n = 1.5$, $St = 2$ without losing generality. The environment temperature is assumed to be much lower than that of the slab, i.e., $\theta_e \cong 0$. Initially the melt is assumed to be superheated at temperature $T_0/T_m = 1.05$. First the results without external convective cooling, i.e., the cases with a pure radiative cooling at the boundary ($H_R = 0$), are presented to illustrate the characteristics of the equilibrium mushy zone solidification of a pure semitransparent material. The effects of various optical parameters, in particular, the optical thickness and the scattering albedo, are investigated in detail. Finally, the effect of external convective heat transfer is presented.

3.1. Thermal characteristics of equilibrium mushy zone solidification

Fig. 2 presents the typical distributions of the temperature and the solid fraction across the slab at various times during solidification for the case with an intermediate value of the optical thickness, $\kappa_D = 5$, and a small conduction–radiation parameter, $N = 0.1$. The scattering effect is not included for simplicity, i.e., $\omega = 0$. Since a local equilibrium condition is employed during solidification, solidification starts when the melt temperature drops to the melting point, i.e., when $\theta = 1$. Since the surface temperature reaches the melting point first, solidification starts at the surface. It is noted that not all of the surface would solidify, however, because of the limited heat removal from the surface by radiation. Instead, only a fraction of the melt at the interface solidified, as evidenced by a solid fraction less than unity at the surface shown in the upper part of Fig. 2 at time $\tau = 0.15$. At that time, the solid fraction at the surface ($x/D = 0$) is only

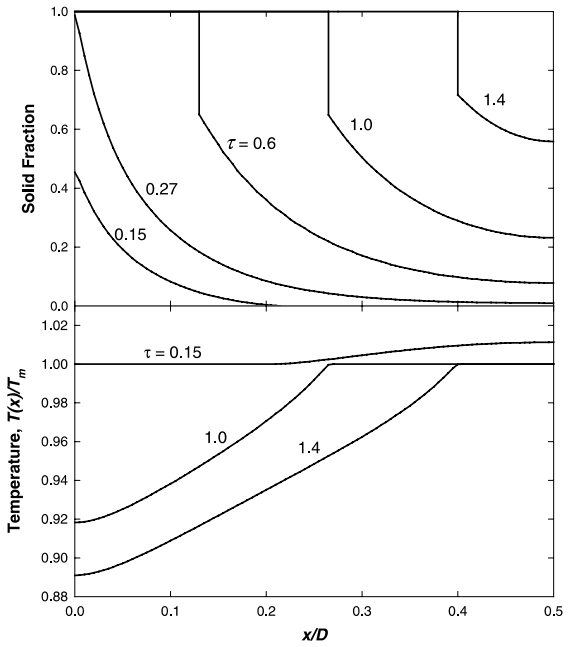

Fig. 2. Solid fraction and temperature distributions across the slab for $\kappa_D = 5$, $N = 0.1$, $\omega = 0$ and $H_R = 0$.

0.46. It is also interesting to notice that the solid fraction, although less than one, extends well into the slab at about $x/D = 0.2$. In other words, a mushy zone is formed immediately when the solidification starts and extends into the layer because of the internal cooling by thermal radiation. Because of the local equilibrium condition, the mushy zone is isothermal at the melting point, as one can see in the temperature distribution curve for $\tau = 0.15$ at the lower part of the figure.

As the solidification takes place, the solid fraction at the surface increases and the mushy zone is also widened. A solid shell is finally formed approximately at $\tau = 0.27$. At that moment, almost the entire slab is in the mushy zone region and the entire slab is at the melting temperature. As solidification goes further, the solid layer temperature drops and the solid shell moves into the slab. Fig. 2 also shows that the solid fraction at the interface is not continuous anymore but undergoes a sudden drop across the solid/mushy zone interface. In the present conditions, it drops fast first to a minimum, and then gradually increases slowly. The sudden drop of the solid fraction at the front of the pure solid region is a result of the discontinuity of the total heat flux at this location. Note that the entire mushy region is at the melting temperature of the material and thus there is no heat conduction in this region; instead, heat is transferred out from the mushy region through internal radiation only, in contrast to the combined mode (heat conduction and radiation) of heat transfer in the solid

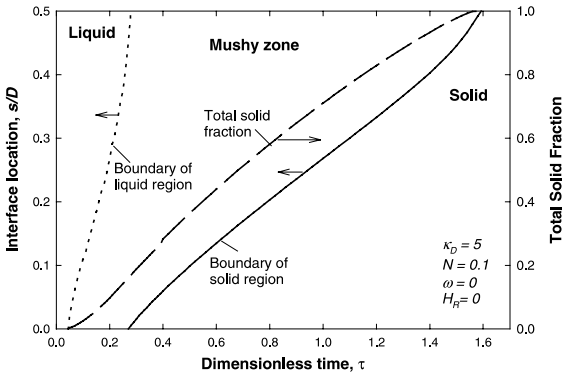

Fig. 3. Locations of the mushy zone boundaries and the total solid fraction as functions of time for $\kappa_D = 5$ with $N = 0.1$, $\omega = 0$, and $H_R = 0$.

region. Because of an exponential feature of radiative heat flux in the mushy region, the variation of the solid fraction is an exponential decay from the interface.

The propagation of the two artificial interfaces, the interface between the solid and the mushy zone and the interface between the mushy zone and the liquid region, is shown in Fig. 3 for the same conditions as in Fig. 2. It can be seen that the pure liquid region shrinks quickly and the mushy zone spreads the entire slab at approximately $\tau = 0.28$, about the same time when a solid shell is formed. Since then, there are only two regions, i.e., the completely solidified layer and the mushy zone. The total solid fraction interface as a function of time is also shown in Fig. 3 as a long dashed line. It can be seen that the long dash and solid lines join each other at the end of solidification. In other words, the mushy zone disappears only at the end of the solidification for this specific case.

3.2. Effects of optical thickness

Figs. 4(a) and (b) present the distribution of the solid fraction in the mushy region at various times for three values of κ_D: 1, 5 and 20, with all other parameters being the same. Fig. 4(a) shows the cases when a solid shell just forms at the surface, while Fig. 4(b) corresponds to the situation when the pure solid front has moved to $X = 0.2$. One can see that the optical thickness of the material has a strong effect on mushy zone solidification. First of all, the optical thickness controls the width of the mushy zone, the larger the value of κ_D, the smaller the mushy zone width. For example, when the solid shell formed at the surface, the mushy zone only extends into the melt at $X = 0.045$ for the case of $\kappa_D = 20$, but the entire slab is in the mushy zone for other two cases with a much smaller κ_D ($\kappa_D = 5$ and 1). Second, the solid fraction at the solid/mushy zone interface is also strongly affected by the optical thickness. As one can see in Fig. 4(b), when κ_D decreases from 20 to 1, the solid fraction at that interface increases from 0.32 to 0.9. This is because a reduced optical thickness increases the internal cooling. Such an increased internal cooling also results in a higher solid fraction in the mushy zone, as illustrated by both cases in Fig. 4.

The solidification time is also strongly affected by the optical thickness. This can be seen in Fig. 4(a). The solid shell forms at $\tau = 0.08$ for $\kappa_D = 20$ but at $\tau = 0.27$ for $\kappa_D = 5$ and at $\tau = 0.93$ for $\kappa_D = 1$. The optical thickness, however, has a mixed effect on the total solidification, as shown more clearly in Fig. 5 which compares the transient locations of the pure solid front and the total solid fraction as a function of time for $\kappa_D = 0.1$, 1 and $\kappa_D = 20$. Under the parameters specified, the total solidification time is the shortest (1.45) for $\kappa_D = 1$ but the longest (3.5) for $\kappa_D = 0.1$. The solidification finishes at an intermediate time duration for the case with the largest optical thickness, $\kappa_D = 20$.

It is also noted in Fig. 5 that the dual lines for $\kappa_D = 0.1$ and 1 are far apart, especially at the earlier times, indicating a widely spread mushy region. For $\kappa_D = 0.1$, solidification takes place in the whole volume during most duration of the solidification process; a completely solidified shell appears only at the end of

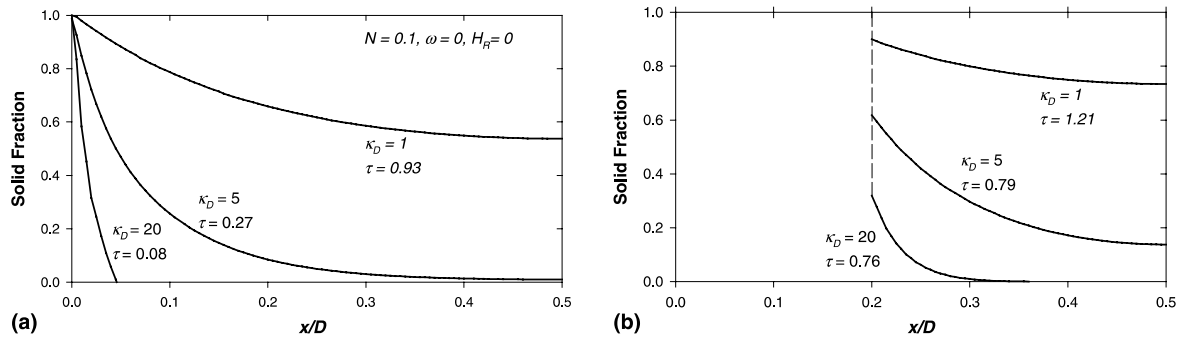

Fig. 4. Solid fraction distributions in the mushy zone for $\omega = 0$, $N = 0.1$, and $H_R = 0$ when the pure solid front reaches approximately (a) $X = 0$ and (b) $X = 0.2$.

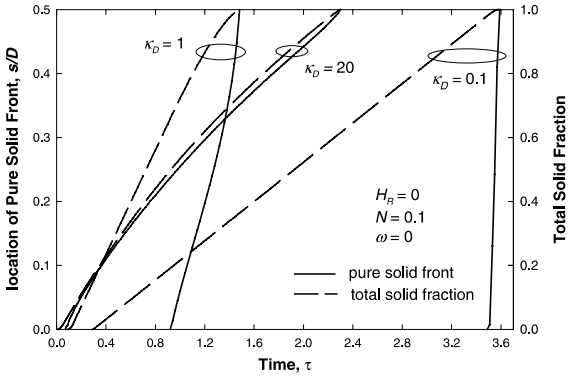

Fig. 5. Locations of the pure solid front and the total solid fraction as functions of time for $\kappa_D = 0.1$, 1 and 20 with $N = 0.1$, $\omega = 0$, and $H_R = 0$.

solidification. For the large optical thickness, i.e., $\kappa_D = 20$, however, the pair lines are very close to each other, implying a narrow mushy region. It is expected that, when one or both of the solid and liquid phases are opaque to radiation, the optical thickness κ_D becomes infinite and the mushy region disappears. This is in agreement with the finding of Chan et al. [15]. The solidification rate is a function of the optical thickness because the heat losses from the slab depend strongly on the optical thickness in the absence of external convection [28].

3.3. Effect of heat conduction

The distributions of the solid fraction in Figs. 2 and 4(b) all show a discontinuity at the boundary between the solid and mushy regions. This is caused by the discontinuous total heat flux at that interface due to the heat conduction in the solid layer but not in the isothermal mushy zone. It is therefore expected that the solid fraction should be a continuous function for the case of pure radiation cooling ($N = 0$). In this case, because the internal radiation is the only mode of heat transfer, the radiative heat flux will be continuous across the pure solid/mushy zone interface under the present assumption of diffusive interface. Fig. 6(a) demonstrates this phenomenon, which presents the solid fraction distributions at various times when the conduction–radiation parameter is zero and all other parameters remain the same as before. As one can see, the solid fraction is 1.0 at the solid/mushy zone interface for all times after a solid shell is formed at about $\tau = 0.27$.

The effect of the heat conduction under the condition of internal radiation can be understood by comparing the variation of the solid fractions under three values of $N = 0, 0.1$, and 0.5, given, respectively, in Figs. 6(a), 4(a), and 6(b). The comparison indicates that the mushy region contains less solidified material or is richer in liquid as heat conduction increases.

3.4. Effect of scattering

The effect of scattering on the mushy zone solidification is examined under different values of optical thickness at $N = 0.1$, $H_R = 0$, and $\kappa_D = 20$ or 5. Three levels of scattering, i.e., $\omega = 0$, 0.9 and 0.99 are considered. The results are in agreement with a previous study [28]. The latter has shown that scattering serves to equalize the temperature distribution and to slow down the transient process. The effects of scattering result in a wider mushy zone and a slower solidification rate, as detailed in the following.

Fig. 7 compares the solid fraction distributions for optical thickness $\kappa_D = 20$ with different scattering levels. Results at two time levels are plotted, i.e., when a solid shell is just formed and when the front of the pure solid has moved to $X = 0.2$. Strong effects of scattering on solidification can be observed immediately. First, scattering reduces the solidification rate and thus increases the solidification time. For example, a solid shell is formed at time $\tau = 0.15$ for the case without scattering, but is formed at $\tau = 0.32$ when the scattering albedo

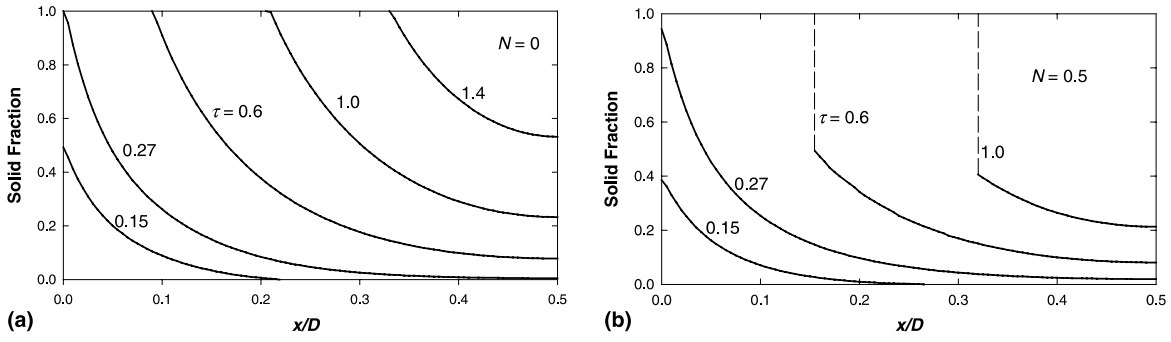

Fig. 6. Effect of heat conduction on the solid fraction distributions in the mushy zone for $\kappa_D = 5$, $\omega = 0$, and $H_R = 0$ with (a) $N = 0$ and (b) $N = 0.5$.

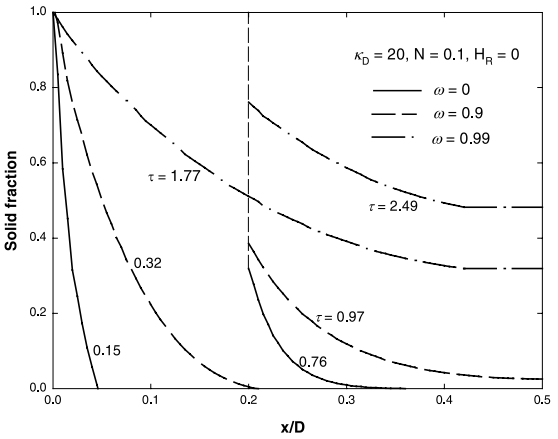

Fig. 7. Effects of scattering on the solid fraction distribution in the mushy zone for $\kappa_D = 20$, $N = 0.1$, and $H_R = 0$ for two locations of the pure solid interface: $X = 0$ and $X = 0.2$.

increases to 0.9. Further increasing the scattering albedo to 0.99, the time needed to form a solid shell at the surface jumps to 1.77. Second, scattering leads to an extended mushy zone with a high solid fraction in the mushy zone. Such an effect of increasing the scattering albedo on the mushy zone solidification process is very similar to that of reducing the optical thickness.

Effects of scattering on the solidification rates can also be understood by examining the propagation of the mushy zone boundaries given by Fig. 8. Fig. 8(a) shows the solid front location and the total solid fraction as functions of time for the same conditions as in Fig. 7. It is easily seen that increasing scattering leads to a wider and a solid-rich mushy zone. Fig. 8(a) also shows the relative variation of the mushy zone width when the scattering albedo increases from 0 (i.e., without scattering) to 0.9 and from 0.9 to 0.99. Such variation demonstrates that scattering has a rather weak effect on solidification unless the scattering strength is very strong, when the optical thickness is large as in the present case.

A much larger effect of scattering exists when the optical thickness is reduced and the internal radiation becomes more important, as shown in Fig. 8(b), which depicts the propagation of the mushy zone boundaries for $\kappa_D = 5$. A rather wide mushy zone is formed when the optical thickness is small as discussed before (solid curves). Scattering further widens the mushy zone. It is interesting to note from Fig. 8(b) that the propagation of the liquid boundary does not change significantly with the scattering strength. The scattering, however, strongly delays the formation of the solid shell and its growth.

3.5. Effect of external convection

External convective cooling is found to have significant effects on the mushy zone behavior, as demonstrated by Fig. 9. Fig. 9(a) shows the propagation of the solidification front at $H_R = 2$ for three optical thickness conditions ($\kappa_D = 0.1$, 1 and 20). Comparing the pairs of curves in Fig. 9(a) with their non-convection (i.e., $H_R = 0$) counterparts in Fig. 5 reveals that addition of external convection leads to a thinner mushy region as well as a faster solidification rate. Indeed, at $H_R = 2$, the total solid fraction interface and the pure solid front line are coincident at the early stage of solidification. This implies that the mushy region is reduced to essentially a planar interface when the interface is close to the boundary surface. Note that at this stage the heat transfer is dominated by conduction due to large temperature gradients in the solid region. Therefore, the solidification rates for different optical thickness in Fig. 9(a) are the same in the beginning. The mushy region gradually emerges later when the role of internal radiation becomes increasingly important with the width depending on the optical thickness. The widest mushy zone is formed for $\kappa_D = 1$, but the mushy zone

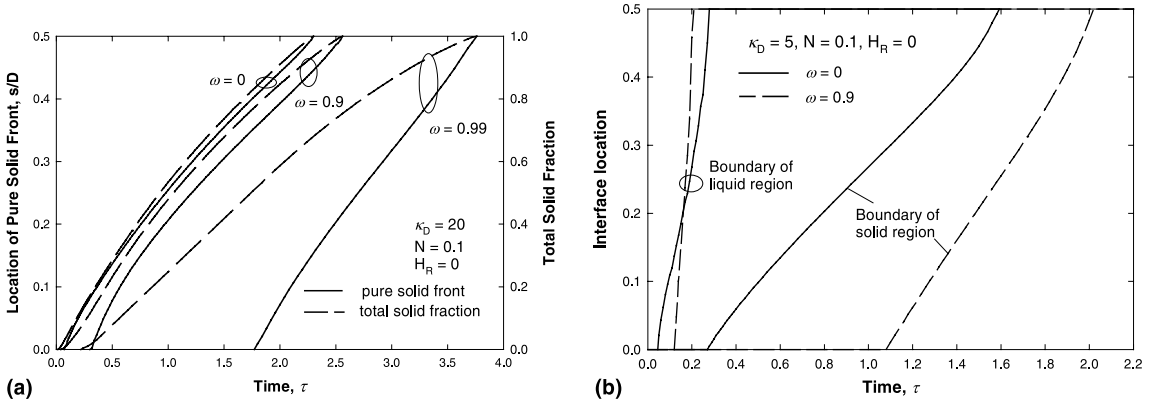

Fig. 8. Effects of scattering on the solidification process for $\kappa_D = 5$ and 20, $N = 0.1$ and $H_R = 0$. (a) Solid front location and total solid fraction for $\kappa_D = 20$. (b) Mushy zone boundary location for $\kappa_D = 5$.

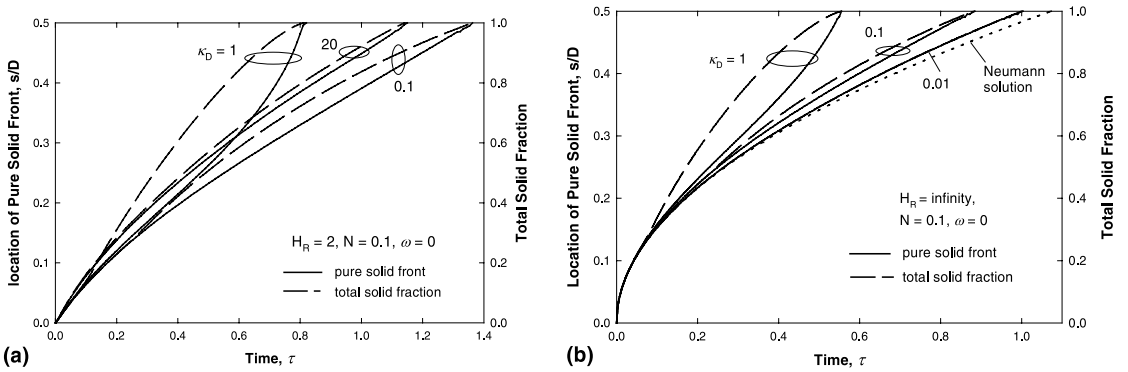

Fig. 9. Transient locations of the pure solid front and the total solid fraction under different external convection conditions for κ_D from 0.01 to 20. (a) $H_R = 2$. (b) $H_R = 1000$ (infinity).

width is significantly smaller than that shown in Fig. 5 for the same optical thickness.

Fig. 9(b) presents some interesting limiting cases. A very large value of H_R is used for the external convection cooling (e.g., $H_R = 1000$). In this case, the boundary condition becomes the first-kind because the surface temperature approaches the ambient temperature (i.e., $T_e = 0$). Several features of the solidification process can be observed from Fig. 9(b). First, similar to what we observed from Fig. 9(a), there is no mushy zone in the early stages of the solidification process due to dominant heat conduction, and the solidification rates in the early stages for all cases are the same regardless the difference in optical thickness. In addition, comparison between Figs. 9(a) and (b) finds that the duration of the planar-interface solidification period is longer for a higher H_R. Second, as κ_D reduces to 0.01, the mushy zone disappears entirely because of negligible internal radiative effect under this condition. In this case, the solidification process can be considered to have a distinct interface between the solid and liquid phases. One can compare this result with the Neumann solution of the classical Stefan problem, i.e., the solidification of a semi-infinite domain with the same initial temperature $T_0/T_m = 1.05$, as given by the dotted line in the figure. It can be seen that a very good agreement exists between the two solutions, at the early stages of solidification. This further demonstrates the soundness of our numerical methods used in this study.

4. Conclusions

This paper presents a systematical study of the mushy zone equilibrium solidification of a one-dimensional pure semitransparent material subject to radiative and convective cooling. It is found that the thickness of the mushy zone and its solid fraction distribution are strong function of the material properties and the external heat transfer conditions. A small optical thickness, a small value of heat conductivity, or a high scattering level all lead to a solid-rich and wider mushy zone. On the other hand, the mushy region disappears when either the material is optically thick or the solidification is at the early stages when there is a strong external convective cooling. Furthermore, the mushy zone also disappears if the material is near transparent so that the internal radiation heat transfer becomes negligible.

Acknowledgements

The research was supported by the Computational Mechanics Research Challenge Grant sponsored by the Ohio Board of Regents. G.-X. Wang would also like to acknowledge the support of the NSF Grant CTS-9711135.

References

[1] R. Viskanta, E.E. Anderson, Heat transfer in semitransparent solids, Adv. Heat Transfer 11 (1975) 317–441.
[2] V.A. Petrov, Optical and thermophysical properties of semitransparent materials in the calculation of combined radiation–conduction heat transfer, Sov. Tech. Rev. B. Herm. Phys. 4 (1993) 1–79.
[3] S. Brandon, J.J. Derby, Internal radiative transport in the vertical bridgman growth of semitransparent crystals, J. Cryst. Growth 110 (1991) 481–500.
[4] S. O'Hara, L.A. Tarshis, R. Viskanta, Stability of the solid–liquid interface of semi-transparent materials, J. Cryst. Growth 3/4 (1968) 583–593.
[5] M. Abrams, R. Viskanta, The effects of radiative heat transfer upon the melting and solidification of semitransparent crystals, J. Heat Transfer 96 (1974) 184–190.
[6] M.G. Vasil'ev, V.S. Yuferev, Influence of radiative heat transfer on the process of growing semitransparent crystals from a melt. I. Radiation supercooling of the melt, Sov. Phys. Tech. Phys. 27 (1982) 779–781.

[7] V.S. Yuferev, M.G. Vasil'ev, Heat transfer in shaped thin-walled semi-transparent crystals pulled from the melt, J. Cryst. Growth 82 (1987) 31–38.
[8] I.S. Habib, Solidification of semitransparent materials by conduction and radiation, Int. J. Heat Mass Transfer 14 (1971) 2161–2164.
[9] N. Seki, M. Sugawara, S. Fukusako, Back-melting of a horizontal cloudy ice layer with radiative heating, J. Heat Transfer 101 (1979) 90–95.
[10] C. Cho, M.N. Ozisik, Effects of radiation on the melting of a semi-transparent, semi-infinite medium, in: Proceedings of the 6th International Heat Transfer Conference, vol. 3, 1978, pp. 373–378.
[11] L.A. Diaz, R. Viskanta, Experiments and analysis on the melting of a semitransparent material by radiation, Warme- Stoffubertrag. 20 (1986) 311–321.
[12] K.S. Kim, B. Yimer, Thermal radiation heat transfer effects on solidification of finite concentric cylindrical medium–enthalpy model and P-1 approximation, Numer. Heat Transfer 14 (1988) 483–498.
[13] I. Nicoara, A. Pusztai, M. Nicolov, On the interface shape of semitransparent crystals obtained by the bridgman method, Cryst. Res. Technol. 32 (1997) 413–422.
[14] G.-X. Wang, C. Yao, B.T.F. Chung, On physical mechanisms of mushy zone formation in solidification of pure semitransparent materials, in: Proceedings of the ASME Heat Transfer Division – 1999, HTD-vol. 364-2, vol. 2, ASME, New York, 1999, pp. 281–288.
[15] S.H. Chan, D.H. Cho, G. Kocamustafaogullari, Melting and solidification with internal radiative transfer – a generalized phase change model, Int. J. Heat Mass Transfer 26 (1983) 621–633.
[16] S.H. Chan, K.Y. Hsu, The mushy zone in a phase change model of a semitransparent material with internal radiative transfer, J. Heat Transfer 110 (1988) 260–263.
[17] V.S. Yuferev, Z. Chvoj, E.N. Kolesnikova, The effect of radiative heat transfer on morphological stability during directional solidification of a binary melt, J. Cryst. Growth 108 (1991) 367–376.
[18] C. Yao, G.-X. Wang, B.T.F. Chung, A non-equilibrium solidification model for semitransparent materials, J. Thermophys. Heat Transfer 14 (2000) 297–304.
[19] F.O. Oruma, M.N. Ozisik, M.A. Boles, Effects of anisotropic scattering on melting and solidification of a semi-infinite semi-transparent medium, Int. J. Heat Mass Transfer 28 (1985) 441–449.
[20] P.M. Beckett, High intensity laser induced vaporization without internal superheating, J. Appl. Phys. 58 (1985) 2943–2948.
[21] V.E. Chizhov, Approximate model of melting of semi-transparent bodies in pulse irradiation, Inzh. Fiz. Z. 63 (1992) 728–736.
[22] R. Siegel, J.R. Howell, Therm. Radiat. Heat Transfer, 3rd ed., Hemisphere, Washington, DC, 1992.
[23] M.F. Modest, Radiative Heat Transfer, McGraw-Hill, New York, 1993 (Chapter 15).
[24] S.V. Patankar, Numerical Heat Transfer and Fluid Flow, Hemisphere, New York, 1980.
[25] W.A. Fiveland, Discrete-ordinates solutions of the radiative transport equation for rectangular enclosure, J. Heat Transfer 106 (1984) 699–706.
[26] C. Yao., Combined heat transfer with melting/solidification in semitransparent materials, Ph.D. dissertation, The University of Akron, Akron, OH, 1999.
[27] R. Siegel, Transient heat transfer in a semitransparent radiating layer with boundary convection and surface reflection, Int. J. Heat Mass Transfer 39 (1996) 69–79.
[28] C. Yao, B.T.F. Chung, Transient heat transfer in a scattering–radiating–conducting layer, J. Thermophys. Heat Transfer 13 (1999) 18–24.